




Highly Efficient, Dual-Functional Self-Assembled Electrospun Nanofiber Filters for Simultaneous PM Removal and On-Site Eye-Readable Formaldehyde Sensing

Jin Yeong Song¹ · Seongmin Kim¹ · Jaeseong Park¹ · Sang Min Park¹ 

Received: 4 October 2022 / Accepted: 21 February 2023 / Published online: 9 March 2023
© Donghua University, Shanghai, China 2023

Abstract

Air pollution containing particulate matter (PM) and volatile organic compounds has caused magnificent burdens on individual health and global economy. Although advances in highly efficient or multifunctional nanofiber filters have been achieved, many existing filters can only deal with one type of air pollutant, such as capturing PM or absorbing and detecting toxic gas. Here, highly efficient, dual-functional, self-assembled electrospun nanofiber (SAEN) filters were developed for simultaneous PM removal and onsite eye-readable formaldehyde sensing fabricated on a commercial fabric mask. With the use of an electrolyte solution containing a formaldehyde-sensitive colorimetric agent as a collector during electrospinning, the one-step fabrication of the dual-functional SAEN filter on commercial masks, such as a fabric mask and a daily disposable mask, was achieved. The electrolyte solution also allowed the uniform deposition of electrospun nanofibers, thereby achieving the high efficiency of PM filtration with an increased quality factor up to twice that of commercial masks. The SAEN filter enabled onsite and eye-readable formaldehyde gas detection by changing its color from yellow to red under a 5 ppm concentrated formaldehyde gas atmosphere. The repetitive fabrication and detachment of the SAEN filter on a fabric mask minimized the waste of the mask while maintaining high filtration efficiency by replenishing the SAEN filters and reusing the fabric mask. Given the dual functionality of SAEN filters, this process could provide new insights into designing and developing high performance and dual-functional electrospun nanofiber filters for various applications, including individual protection and indoor purification applications.

Keywords Electrospinning · Nanofiber · Self-assembly · PM removal · Formaldehyde sensing

Introduction

Air pollution has steadily increased over the past decades and has become a substantial burden on the global environment and the health of humankind beyond the environmental concerns of cities and countries [1–6]. As a by-product of rapid industrialization and population growth, particulate matter (PM) and toxic gases are major sources of air pollutants and have caused various cardiac and respiratory diseases upon short- or long-term exposure [7–11]. Also known as airborne solid/liquid droplets or aerosols, PM

is defined as fine and ultrafine particles and is composed of ionic, metal, and carbon mixtures [12–14]. Toxic gases are invisible and colorless and are composed of exceptionally complex gaseous substances such as CO, NO₂, HCHO (formaldehyde), and volatile organic compounds (VOCs) [15, 16]. With technological advancement, various filtration equipment or sensing methods for PM and toxic gases have been explored; however, individuals are still exposed to these threats in daily life and work [17–22].

PM filtration is commonly performed with conventional filters made of chemically synthesized or petroleum-based materials [23]. Filtration is mainly accomplished through physical PM size-based trapping mechanisms, including sieving, blocking, diffusion, and electrostatic attraction [24]. Among various methods to fabricate air filters, electrospinning has been studied with great interest owing to its intriguing ability to fabricate nanofiber filters with controllable permeability and high porosity and using various choices

✉ Sang Min Park
sangmin.park@pusan.ac.kr

¹ School of Mechanical Engineering, Pusan National University, 63-2 Busan University-Ro, Geumjeong-Gu, Busan 46241, South Korea

of materials [25–31]. With these beneficial properties, various electrospun nanofiber filters have been developed with improved PM removal efficiency, breathable pressure drops, and lighter base weight compared with conventional filters produced by other processes [32–39]. Owing to their mechanical properties, nanofibers are fragile to be utilized standalone as air filters. Hence, a nanofiber mat is frequently used as air filter after being transferred to the frames or substrates by transfer processes, including roll-to-roll transfer [40, 41]. For the simplified fabrication of air filter, the direct fabrication of an electrospun nanofiber mat onto an electroconductive substrate, such as window screens, was developed without the transfer [42–45]. As an extension of the direct fabrication of a nanofiber filter on the conductive substrate, the non-conductive substrate should be studied for practical use because air filters are generally composed of non-conductive materials, such as daily masks and industrial air filters [46–48].

Traditional toxic gas removal is mainly performed with an adsorption framework, such as a half- or full-face respirator, to selectively absorb gases from air pollutants [49–51]. However, many gas absorbers have a limited allowable gas concentration, and wearing a half- or full-face respirator is uncomfortable in daily life [52, 53]. Thus, recognizing the state of toxic gas in daily life would greatly reduce the potential risk of toxic gas [54]. Many researchers have developed toxic gas sensing devices, including chromatographic and colorimetric sensors, to alarm against the existence of toxic gases [55–57]. Chromatographical sensors enable high-precision detection of toxic gases but require high-cost equipment and a controlled environment for the measurement [58–60]. Colorimetric sensors exhibit rapid color changes by reacting with toxic gases without requiring any expensive equipment, thus placing them in the spotlight with their onsite eye-readable sensing ability [61–63]. Among various toxic gas sensors, nanofiber-based toxic gas sensors have shown great promise in detecting toxic gases with high-speed and superior precision owing to their high reactive surface area [64–66]. Nanofiber filters have exhibited excellent performance in treating one type of air pollutant, including gas sensing and PM removal. With the wide spread of complex air pollution, including combinations of pathogens such as COVID-19 virus, PM, and toxic gases, dual-functional air filters that can simultaneously capture PM and detect gases are required from daily and industrial points of view.

In this study, we suggested highly efficient, self-assembled electrospun nanofiber (SAEN) filters for simultaneous PM removal and eye-readable onsite formaldehyde detection. The premise of our design is a facile one-step fabrication of dual-functional nanofiber filters that could capture PM and detect formaldehyde gas simultaneously by utilizing an electrolyte solution containing a formaldehyde-sensitive

colorimetric agent. Given that the electrolyte solution can act as a sacrificial collector in electrospinning [46], electrospun nanofibers can be directly deposited onto a non-conductive mesh collector and self-assembled in a uniform distribution to be fabricated as a SAEN filter without post-processing or transfer process. The SAEN filters exhibited higher $PM_{2.5}$ filtration efficiency and similar pressure drops, leading to higher quality factors than commercial masks. Meanwhile, the repetitive fabrication and detachment of SAEN filters showed the potential for waste reduction based on the lower weight of SAEN filters compared to fabric or commercial masks. Next, the eye-readable formaldehyde detection of the dual-functional SAEN filter was confirmed with its gradual color change of the SAEN filter from yellow to red under formaldehyde gas, which is a representative indoor VOC. This formaldehyde detection was simultaneously performed with PM removal, and thus dual-functional SAEN filters for PM capture and real-time eye-readable formaldehyde sensing were successfully demonstrated.

Experimental

Materials

Gelatin powder from bovine skin (GEL, type B), polycaprolactone (PCL, $M_n \sim 80,000$), poly(vinylidene fluoride) (PVDF, $M_w \sim 275,000$), polystyrene (PS, $M_w \sim 280,000$), nylon 6/6 (NY) were selected as the solute of electrospinning solution and denoted as NY, PCL/GEL, PVDF, and PS, respectively. N, n-dimethylformamide (DMF, $\geq 99.9\%$), 2,2,2-trifluoroethanol (TFE, $\geq 99.0\%$), formic acid ($\geq 98.0\%$), chloroform ($\geq 99.5\%$), methanol ($\geq 99.5\%$), and acetone ($\geq 99.7\%$) were utilized for the solvent of electrospinning solution. All solutes and solvents were provided from Sigma–Aldrich (USA). Tetrabutylammonium bromide (TBAB, $\geq 99.0\%$) was also obtained from Sigma–Aldrich (USA). Potassium chloride (KCl, $\geq 99.0\%$) and deionized (DI) water were acquired from Duksan Chemical Co., Ltd. (South Korea). Sylgard® 184 polydimethylsiloxane (PDMS) silicone elastomer base monomer and hardener were bought from Dow Corning (USA). All ingredients and materials were utilized without further purification.

Preparation of Polymer Solutions for the Electrospinning Process

PCL/GEL solution was prepared by stirring PCL and GEL solution at a 1:1 mass ratio for 12 h with 10 μ L of acetic acid to obtain a homogeneous and transparent state of the solution. PCL and GEL solutions were obtained by stirring PCL pellets and GEL powder at a 10 w/v% in TFE solvent for 12 h, respectively. NY pellets were dissolved in formic

acid for 6 h to obtain 15 wt% NY solution. PVDF pellets were added to a mixture of acetone and DMF (3:7 volume ratio) with stirring for at least 12 h at 60 °C or higher to produce a 25 wt% PVDF solution. PS pellets and DMF solution with 0.05 w/v% of TBAB were mixed for 6 h to generate a 15 w/v% PS solution.

One-Step Fabrication of Dual-Functional SAEN Filters

A 3 mL plastic syringe with one of the four types of polymer solutions was placed in a NE-1000 syringe pump (New Era Pump Systems, Inc., USA), which ejected the polymer solutions through a 23-gauge metal needle with an inner diameter of 0.337 mm at a flow rate of 0.4 mL h⁻¹. Non-conductive mesh collectors, such as a fabric mesh or polypropylene (PP) wiper, were treated using a plasma equipment (CUTE, Femto Science, South Korea) with a consistent plasma power of 100 W, an airflow rate of 20 ccm, and a plasma time of 180 s. The plasma-treated non-conductive mesh collector was immersed in an electrolyte solution for electrolyte-assisted electrospinning [46]. For the direct fabrication of dual-functional SAEN filters, the electrolyte solution was prepared by mixing 15 mL of DI water with 0.5 g of hydroxylamine sulfate, 0.01 g of methyl yellow, 2.5 mL of glycerin, and 32.5 mL of methanol. For the complete immersion of the mask, the solution was prepared using the mixing ratio of the formaldehyde-sensitive solution. An electrolyte solution of 0.3 mol KCl solution was also utilized to investigate the influence of the electrolyte solution on the direct fabrication of a SAEN filter onto the non-conductive mesh collector. The electrolyte-solution-socked mesh collector on a polymethyl methacrylate plate was positioned 20 cm directly under the metal needle. The HV30 power supply (NanoNC Co., Ltd., South Korea) delivered 21 kV between the metal needle and the mesh collector for electrospinning. Electrospun nanofibers were deposited on the electrolyte-solution-socked mesh collector and formed into a SAEN filter. The electrospinning time for each SAEN filter made of PCL/GEL, NY, PVDF, and PS was set to 4, 5, 1, and 2 min, respectively. Except for electrospinning time, other experimental conditions remained constant. The SAEN filters made with different polymer solutions of NY, PCL/GEL, PVDF, and PS solution were named SAEN-NY, SAEN-PCL/GEL, SAEN-PVDF, and SAEN-PS filters, respectively. The SAEN-NY filter was selected for the fabrication of the dual-functional SAEN filter, spontaneously immersed in the electrolyte solution during electrospinning, and dried in a vacuum chamber for 1 h to remove excess electrolyte solution. Finally, a dual-functional SAEN filter was obtained.

Characterization of SAEN Filters

The morphology of SAEN filters was visualized by scanning electron microscope (SEM), and the diameter of the nanofibers was quantified from the SEM image by ImageJ. The SAEN filters were immersed in the uncured PDMS mixture of the PDMS monomer and hardener (10:1 mass ratio), and the uncured PDMS mixture was cured in a dry oven at 50 °C for 12 h. The SAEN filters were embedded in PDMS and cross-sectioned; the thickness of the SAEN filters was measured based on the cross-sectional image captured by a microscope (BX53, Olympus, Japan).

Numerical Simulation

A direction of electric field expressed between the metal needle and mesh collector systems was numerically calculated by COMSOL Multiphysics v5.0 (USA) software. The cross-sectional rendered image of the mesh collector, which was assumed as a fabric mesh, was adopted for 2D numeric simulation with or without the electrolyte solution. Other electrospinning parameters were designated as the experimental conditions of electrospinning: (1) 20 cm distance between the metal needle and the collector system and (2) 21 kV electrical potential. The electrolyte solution was absorbed by the mesh collector and modeled according to the space charge density of the interstitial electrolyte solution in the mesh collector. Mobile ions in the electrolyte solution can be described by the Boltzmann equation, resulting in the space charge density $\rho(x)$, as follows:

$$\rho(x) = -2ec_0 \sinh\left(\frac{e}{k_B T} \varphi(x)\right), \quad (1)$$

where e is the electron charge (J), c_0 is the electrolyte concentration (mmol L⁻¹), k_B is the Boltzmann's constant (J K⁻¹), T is the temperature (K), and φ is the electric potential (V) [67]. The dielectric constant of the electrolyte solution of 0.3 mol KCl solution was set as 80. The curved interface between air and electrolyte solution with different contact angles from 45° to 90° was examined to investigate the influence of air-electrolyte solution interfaces on electric field. The direction of the electric field was displayed along the reference line $\rho(x)$ above the mesh collector.

Air Filtration Efficiency, Pressure Drop, and Air Permeability Measurement

A schematic and an actual image of an experimental setup for the air filtration test are presented in Fig. S1. An electrospun nanofiber filter on the mesh collector was installed in the middle of two glass chambers. PM counter sensors,

which measure the PM density of the air in real time, were installed on both sides of the chamber. Before the experiment, the fan mounted on the left side of the chamber produced constant airflow, and PM was continuously produced by burning incense from the right side to the left side of the chamber. The generated PM has a broad size distribution of over 300 nm to below 10 μm , and the majority are below 1 μm in size [68]. PM densities from the inlet and outlet of the chamber system were measured by a PM counter sensor module (Wuhan Cubic Optoelectronics Co. Ltd., PM2008) with the simultaneous detection of $\text{PM}_{0.5}$, $\text{PM}_{1.0}$, $\text{PM}_{2.5}$, $\text{PM}_{5.0}$, and PM_{10} . $\text{PM}_{2.5}$, $\text{PM}_{1.0}$, and $\text{PM}_{0.5}$ were utilized to measure the air filtration performance. Airflow was fixed to 0.11 m s^{-1} by controlling the power of the fan. Each air filtration test was conducted for 5 min by each polymeric nanofiber filter fabricated with or without the electrolyte solution. Electrospun nanofiber filters fabricated with or without the electrolyte solution on the fabric mesh or PP wiper were placed in the middle neck of the custom chamber system with 23 mm diameter to evaluate the filtration efficiency and pressure drop during air filtration. A differential pressure manometer (DT-8890A, CEM Instruments, China) was utilized to measure the pressure drop during the test. Airflow was varied by 0.055, 0.165, and 0.22 m s^{-1} to examine the influence of airflow velocity on PM filtration efficiency and pressure drop of each filter. Pressure drop was also measured during the PM filtration test. Air permeability was evaluated in accordance with ISO 9237 standard via FX-3300 LabAir IV (TEXTTEST AG, Switzerland) under 100 Pa applied pressure, 50% relative humidity (RH), and room temperature of 25 $^{\circ}\text{C}$ with 5 cm^2 of KF94 mask, fabric mesh or mask, and electrospun nanofiber filters fabricated with or without the electrolyte solution.

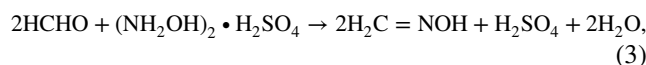
Formaldehyde Detection with Dual-Functional SAEN Filters

The dual-functional SAEN filter was placed in a 3.3 L testing chamber with a room temperature of 25 $^{\circ}\text{C}$ and RH of 40–50%. The concentration of formaldehyde in the chamber was calculated in ppm as follows:

$$C = \left(\frac{22.4\rho_f TV_f}{273M_f V} \right) \times 10^3, \quad (2)$$

where C is the formaldehyde concentration, ρ_f is the density of liquid formaldehyde, T is the temperature in the chamber, V_f is the volume of liquid formaldehyde, M_f is the molecular weight of formaldehyde, and V is the chamber volume. Air Quality sensor (PAQUAT, ~ 10 ppm, Wujing HighTech Co., Ltd) was utilized to detect the concentration of formaldehyde gas reached and maintained at 5 ppm in the chamber within the short-term exposure limit of formaldehyde gas

concentration (2 ppm) in accordance with OSHA standards. In the formaldehyde detection test, the dual-functional SAEN filter was exposed to formaldehyde gas for 30 min. The formaldehyde gas reacted with hydroxylamine sulfate in the SAEN filter, producing sulfuric acid that altered the color of methyl yellow from yellow to red, which could be identified by the naked eye. The reaction to this process is represented as follows:



The color change of the dual-functional SAEN filter was captured every 5 min from the original state by a DSLR camera (EOS-M50, CANON, Japan) during experiments. Captured images were verified qualitatively by visual inspection and quantitatively converted into RGB (red, green, and blue) values by Image J. The different concentrations of formaldehyde gas, such as 0, 100, 200, 500, 1,000, 2,000, and 5,000 ppb, were adopted to explore the formaldehyde reaction-dependent RGB color change furtherly. Finally, the relationship between PM filtration and formaldehyde gas detection of the dual-functional SAEN filter was verified through PM filtration after reacting with a 5 ppm concentration of formaldehyde gas per 5 min. The fabricated dual-functional SAEN filters on commercial masks were secured at room temperature and 40% of RH for 1, 2, and 3 weeks and utilized for PM filtration and formaldehyde sensing to investigate their service time.

Results and Discussion

One-Step Fabrication of Dual-Functional SAEN Filters for Simultaneous PM Removal and Formaldehyde Sensing

Figure 1a demonstrates the respiratory configuration during the use of a dual-function SAEN filter when exposed to contaminated air containing PM and formaldehyde gas. The dual-functional SAEN filter can effectively remove PM in the air to allow fresh air intake through the human respiratory system and simultaneously detect formaldehyde gas by altering its color from yellow to red. Figure 1b shows the schematic of the overall fabrication of the dual-functional SAEN filter onto non-conductive mesh collectors for PM capturing and formaldehyde gas sensing. The one-step fabrication of dual-functional SAEN filters on non-conductive mesh collectors could be achieved by utilizing an electrolyte solution containing a formaldehyde-sensitive colorimetric agent as a conductive collector for electrolyte-assisted electrospinning. Among various collectors, a dual-functional SAEN filter on a commercial daily air filter mask was used to demonstrate its potential

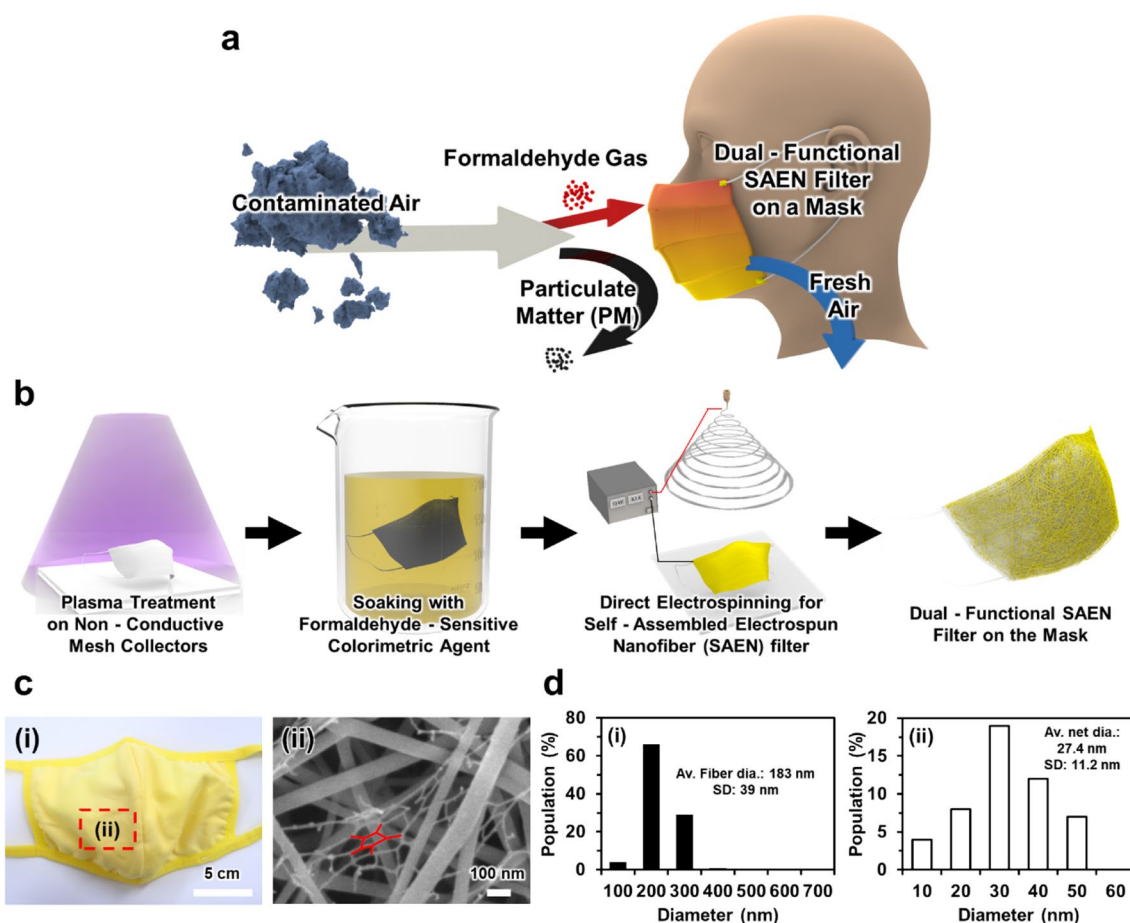


Fig. 1 **a** Schematic diagrams of dual-functional self-assembled electrospun nanofiber (SAEN) filter for PM removal and formaldehyde gas sensing from contaminated air. **b** One-step fabrication process of dual-functional SAEN filter by direct electrospinning on a plasma-treated commercial filter soaking in an electrolyte solution containing

as a daily wearable device. Commercial fabric (cotton) and polymer (polypropylene, PP) masks were adopted as commercial daily air filters. Before the direct fabrication of the SAEN filter on a mask, plasma treatment was performed to modify the wettability of the mask to be hydrophilic. The plasma treatment generated uniform hydroxyl groups ($-OH$) on the surface of the mask, thereby rendering the surface hydrophilic regardless of its materials. This hydrophilic surface facilitated the absorption of electrolyte solution into the plasma-treated mask. Afterward, the plasma-treated mask was soaked in the electrolyte solution and subjected to direct electrospinning to fabricate the SAEN filter onto the electrolyte solution-soaked mask. Given that an electrolyte solution could act as the sacrificial electroconductive collector [46], electrospun nanofibers were deposited onto the surface of the electrolyte solution-soaked mask composed of the non-conductive fabric or polymer. The electrolyte solution covered

the formaldehyde-sensitive colorimetric agent. The front view (**c-(i)**) and SEM image (**c-(ii)**) of a dual-functional SAEN filter on a fabric mask. Scale bars are 5 cm (**c-(i)**) and 100 nm (**c-(ii)**), respectively. The diameter population of nanofibers (**d-(i)**) and nanonets (**d-(ii)**) in a dual-functional SAEN filter

the mask, and electrospun nanofibers were deposited and self-assembled on the surface of the electrolyte solution by the force balance between the electrostatic attraction force and the surface tension of the electrolyte solution, thereby forming a SAEN filter over the entire surface of the mask. During electrolyte-assisted electrospinning, the electrolyte solution containing a formaldehyde-sensitive colorimetric agent enabled the formation of a self-assembled nanofiber filter on the mask and simultaneously impregnated the formaldehyde-sensitive colorimetric agent onto the SAEN filters. After drying, the SAEN filter could capture PM and detect trace amounts of formaldehyde gas by colorimetric change.

The fabricated dual-functional SAEN filter is exhibited in Fig. 1c-(i). Given that the mask and the SAEN-NY filter were immersed in the formaldehyde-sensitive colorimetric agent, no difference in color was found between them. The red rectangular region was enlarged to show the SEM image of a

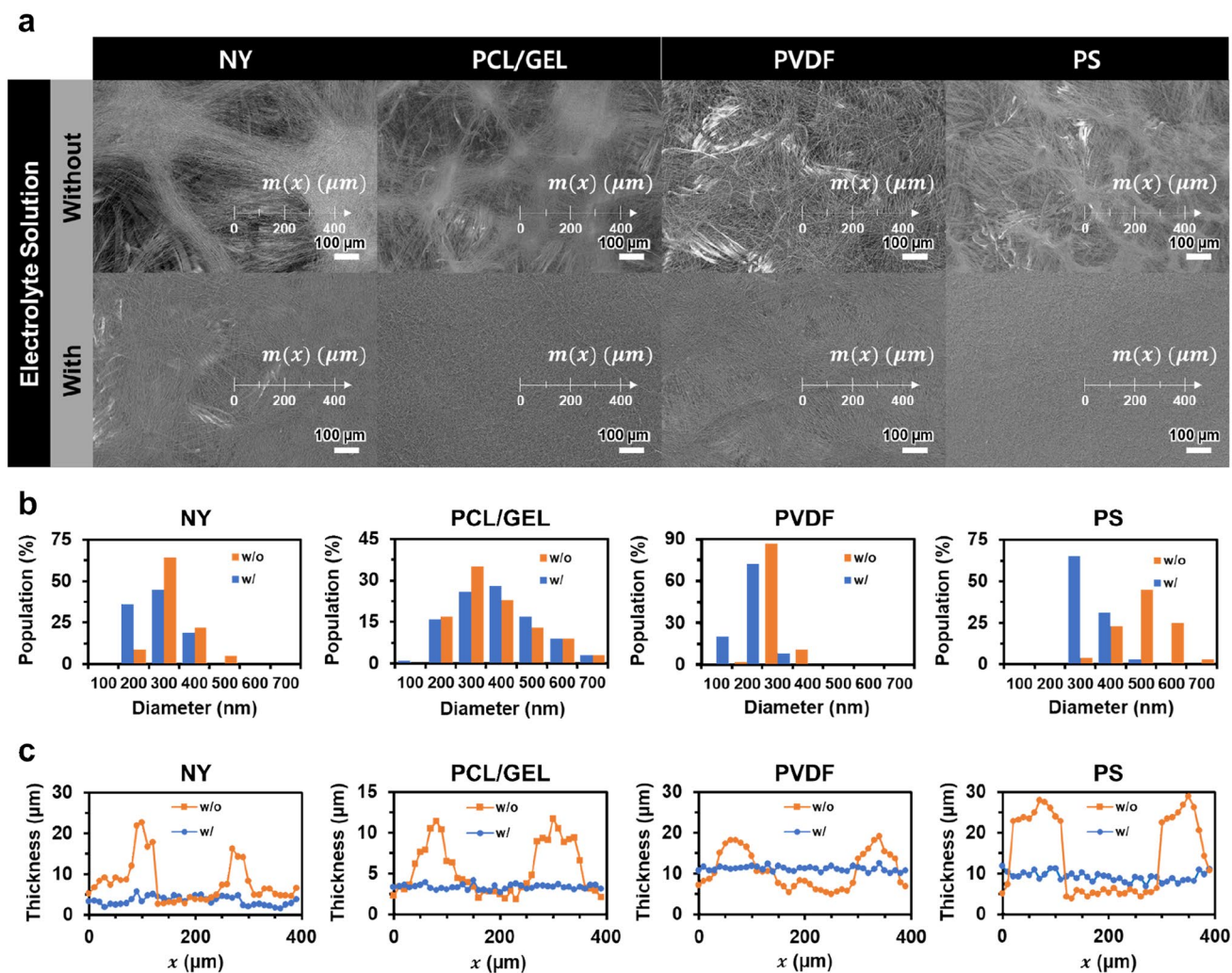


Fig. 2 SEM images (a), diameter distributions (b), and thickness (c) of electrospun nanofiber filter fabricated with or without the electrolyte solution on the fabric mesh with four different polymers (NY, PCL/GEL, PVDF, and PS). All scale bars are 100 μm

dual-functional SAEN filter in Fig. 1c-(ii). Randomly oriented NY nanofibers and spider-web-like structures called nanonets were observed in the dual-functional SAEN filter. Figure 1d-(i) and (ii) exhibit the diameter range of nanofibers and nanonets with averages of 183 ± 39 and 27.4 ± 11.2 nm, respectively. Nanofiber filters with nanonets feature controllable permeability, various choices of materials, and intriguing features (e.g., Steiner-tree network geometry and extremely small diameter), which enable high performance or functional filtration for ultrafine PM or viruses. Many researchers reported that nanonets could possess high interconnectivity and additional surface area, resulting in fast analyte diffusion [69–71]. Thus, the nanofiber filters with nanonets could be alluring candidates as air filters that can simultaneously capture PM and sense gaseous materials.

Direct Electrospinning of SAEN Filters onto a Non-Conductive Mesh Collector

The direct fabrication of electrospun nanofiber filters on a non-conductive mesh collector with or without the electrolyte solution was investigated. Figure 2a shows the SEM images of the electrospun nanofiber filter fabricated with or without the electrolyte solution. In the absence of the electrolyte solution, the electrospun nanofiber filters composed of PCL/GEL, NY, PVDF, and PS exhibited non-uniform density and locally concentrated regions of electrospun nanofibers (Fig. 2a). The non-uniform density of electrospun nanofibers was attributed to the microfibrinous structure of the non-conductive mesh collector. Such microfibrinous structures of the collector aggregated the electrospun nanofibers to cause non-uniform deposition, even with non-conductive collectors [72, 73].

By contrast, electrospun nanofibers fabricated with the electrolyte solution self-assembled on the surface of the electrolyte solution, and thereby, a uniformly distributed SAEN filter was exhibited on the non-conductive mesh collector. As shown in Fig. 2b, the declining tendency of diameter distribution of nanofibers did not show significantly between electrospun nanofibers filters fabricated with or without the electrolyte solution, rather the smaller diameter of nanofiber filters is generally known to enhance the surface-to-volume ratio, which provides higher PM filtration efficiency by sieving and adhesion for smaller PM. For the quantitative comparison, the thickness of the SAEN filter and electrospun nanofiber filter fabricated without the electrolyte solution were measured along reference line $m(x)$ indicated in Fig. 2a (c). Interestingly, the thick regions of the electrospun nanofiber filter fabricated without the electrolyte solution coincided with the ridge of the fibrous structure of the mesh collector. Furthermore, the thin regions of the electrospun nanofiber filter fabricated without the electrolyte solution were observed in the voids of the non-conductive mesh. In contrast, all SAEN filters had a uniform thickness regardless of the deposited location of SAEN filters.

For further analysis of the SAEN filters, the cross-sectioned morphology of the SAEN filter and electrospun nanofiber filter fabricated on the non-conductive mesh collector without the electrolyte solution are shown in Fig. 3. Electrospinning without the electrolyte solution on the non-conductive mesh collector generated a non-uniform electrospun nanofiber filter mainly on the fibrous structure of the mesh collector (Fig. 3a-(i)). Meanwhile, electrolyte-assisted electrospinning produced electrospun nanofibers that were self-assembled on the surface of the electrolyte solution and formed into a uniformly distributed SAEN filter on top of the mesh collector (Fig. 3a-(ii)). For the study of thickness of the SAEN filter and electrospun nanofiber filter fabricated without the electrolyte solution, the cross-section image of each sample embedded in PDMS are shown in Fig. 3b-(i) and (ii),

respectively. As displayed in Fig. 3b-(i), the electrospun nanofiber filter fabricated without the electrolyte solution exhibited the locally thick regions. Meanwhile, Fig. 3b-(ii) shows a uniformly distributed SAEN filter throughout the non-conductive mesh collector. Considering the various factors that are applied to electrospinning, the polymer type would influence the deposition behavior of electrospun nanofibers. However, the deposition behavior of electrospun nanofibers was mainly governed by inertia and electrostatic force, not the type of polymer. Thus, with appropriate electrospinning conditions, including concentration, flow rate, applied voltage, and distance, for each polymer type, the SAEN filter could be successfully fabricated on the collector with uniform thickness. These observations indicated that the SAEN filter would possess a uniform thickness regardless of the polymer type and the topography of the collector.

Numerical Simulation of Electrospinning with or Without the Electrolyte Solution

Given that the deposition of electrospun nanofibers is generally determined by the electrostatic attraction between the charge of electrospun nanofibers and the electric field, the deposition of electrospun nanofibers on the mesh collector system was investigated by the numerical simulation of the electric field. Figure 4a-(i) illustrates the configuration of the electrospinning process with the mesh collector system. The assumption was that the mesh collector had a microfibrillar structure, and electrolyte solution totally covered the mesh collector. In practice, the electrolyte solution can wet the fibers and exhibit sagging air-liquid interfaces due to capillary forces. Considering that the contact angle and the capillary force are varied according to the type of materials and plasma treatment [76], curved air-electrolyte solution interfaces were estimated based on the different contact angles from 45° to 90° . The direction and average intensity of the electric field on the mesh collector were visualized by the direction and size of the red arrow, respectively, along

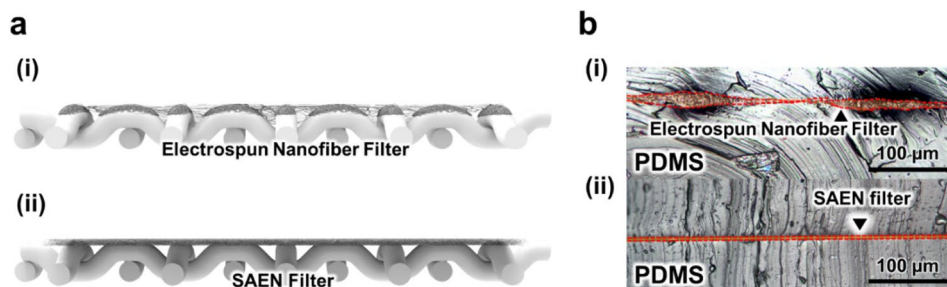


Fig. 3 A cross-sectioned morphology of the electrospun nanofiber filter fabricated without the electrolyte solution (**a-(i)**) and the SAEN filter (**a-(ii)**) on the non-conductive mesh collector. PDMS-embedded

cross-sectional image of the SAEN filter (**b-(i)**) and the electrospun nanofiber filter fabricated without the electrolyte solution (**b-(ii)**). Scale bars are 100 μm

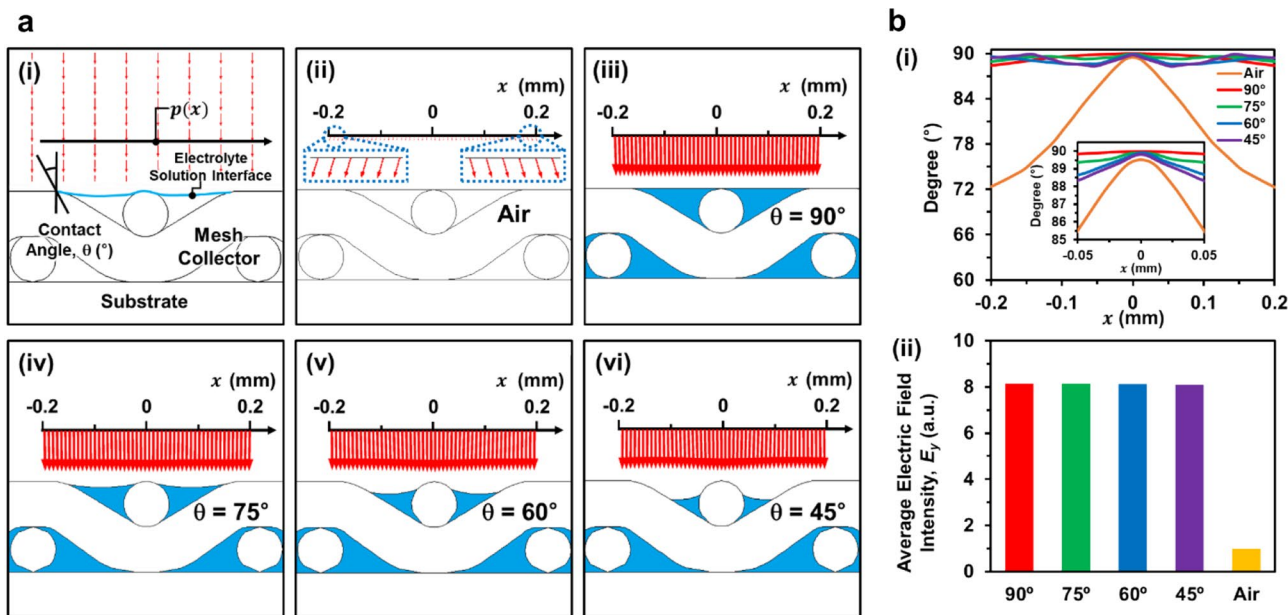


Fig. 4 (a-(i)) The simulated direction of the electrostatic field for a mesh collector system. Electrostatic field distribution toward the mesh collector without (a-(ii)) or with the electrolyte solution with different contact angles of 90° (a-(iii)), 75° (a-(iv)), 60° (a-(v)), and 45° (a-(vi)) along the reference line $p(x)$. Inset of (a-(ii)): The magnified electric field toward the mesh collector without the electrolyte

solution. The direction of the electric field (b-(i)) and average electric field intensity (E_y) (b-(ii)) to the mesh collector system with or without the electrolyte solution with different contact angles along the reference line $p(x)$. Inset of (b-(i)): The magnified image of the direction of the electric field

an imaginary line $p(x)$. As shown in Fig. 4a-(ii) and (iii), the electric field was concentrated toward the ridge of the microfibrillar structure of the mesh collector for the case without the electrolyte solution but was evenly distributed toward the whole region of the mesh collector for the case with the electrolyte solution. Also, the average electric field intensity (E_y) for the mesh collector without the electrolyte solution was much smaller than that of the mesh collector totally covered with the electrolyte solution. Owing to the polarization of the non-conductive mesh collector, the electric field was focused toward the ridge of the microfibrillar structure for the case without the electrolyte solution, as shown in Fig. 4a-(ii) [74, 75]. For the case of the electrolyte solution, the electrolyte solution totally covered the non-conductive mesh collector and generated a uniformly distributed electric field toward the surface of the electrolyte solution, as shown in Fig. 4a-(iii-vi). The presence of electrolyte solution dramatically increased the uniformity of the direction and intensity of the electric field toward the mesh collector. In Fig. 4b-(i) and (ii), the direction and average intensity of these electric fields are compared with or without electrolyte solution with different contact angles. The electric field was evenly distributed along the reference line $p(x)$ in the presence of electrolyte solution rather than without electrolyte solution, while a slight variation in the electric field was observed between the electric field under different contact angles.

Furthermore, using an electrolyte solution could increase the average intensity of the electric field concentrated toward the mesh collector. On the basis of these results, the electrospun nanofibers would be uniformly deposited with the help of the electrolyte solution, even though the mesh collector had topographies of the microfibrillar structure.

PM Filtration Efficiency, Pressure Drop, and Air Permeability of SAEN Filters

Figure 5a shows a schematic of air filtration with an electrospun nanofiber filter and SAEN filter onto the fabric mask in contaminated air. Based on previous observations and simulation results, large pores or voids were observed on the electrospun nanofiber filters fabricated without electrolyte solution (Fig. 5b). In contrast, the SAEN filter was found to be uniformly formed throughout cotton fibers (Fig. 5c). Figure 5b, c display the air filtration mechanism of electrospun nanofiber filter with or without electrolyte solution, respectively. PM can be filtered through adhesion and sieving due to inertial deposition, blocking, electrostatic deposition, and diffusion [24]. However, the electrospun nanofiber filter fabricated without electrolyte solution can pass PM due to the existence of large pores or voids. On the other hand, the SAEN filter, possessing uniform thickness, could effectively filter PM by sieving and adhesion. Furthermore,

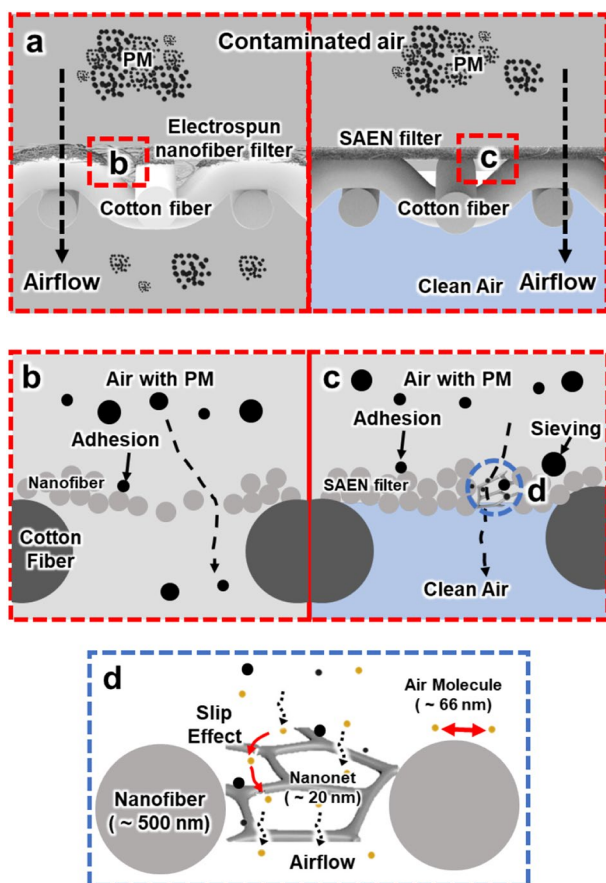


Fig. 5 a Schematic of air filtration with electrospun nanofiber filter fabricated without electrolyte solution and SAEN filter. Filtration mechanism, including sieving and adhesion, with electrospun nanofiber filters without electrolyte solution (b) and SAEN filters (c), and the mechanism of the slip effect of airflow by nanonets (d)

considering that the SAEN-NY filter exhibited nanonets with their extremely small diameter (~ 20 nm) that is smaller than the mean free path of air molecules (~ 66 nm), nanonets could enhance the slip effect of air, leading to a decrease in pressure drop (Fig. 5d) [41].

Figure 6a shows the $PM_{2.5}$ filtration efficiency of the SAEN filter and electrospun nanofiber filter fabricated without the electrolyte solution. Given that the filtration efficiency increases with the thickness of the electrospun nanofiber filter, a thick electrospun nanofiber filter is effective in terms of filtration. Thus, electrospinning time was empirically determined for the SAEN filter to reach its $PM_{2.5}$ filtration efficiency comparable with that of a KF94 mask. In Fig. 6a, the SAEN filters demonstrated superior $PM_{2.5}$ filtration efficiency over the fabric mesh. In addition, the $PM_{2.5}$ filtration efficiency of the SAEN filter was higher than that of the electrospun nanofiber filters fabricated without the electrolyte solution over at least a 3–15% increase with the same electrospinning time. These enhanced $PM_{2.5}$ filtration

of the SAEN filters were similar to or higher ($> 97.99\%$) than that of KF94 mask (97.86%). As another critical factor of air filtration filters, pressure drops were also measured during the air filtration test. The measured pressure drops of the SAEN filter and the electrospun nanofiber filter fabricated without the electrolyte solution are presented in Fig. 6b. The absence of the electrolyte solution in the fabrication of the electrospun nanofiber filter did not significantly affect the pressure drops, and all measured pressure drops were similar or lower than that of the KF94 mask. Quality factor (QF), a measure of air filtration performance based on filtration efficiency and pressure drop, was calculated as follows:

$$QF = \frac{-\ln P}{\Delta p}, \quad (4)$$

where P is the ratio of the penetration rate of PM, and Δp is the pressure drop across the filter media. Here, P is equivalent to $1-E$, where E is the PM filtration efficiency of the filter media. A large QF value represents the high performance of the filter. Figure 6c compares the QF values by $PM_{2.5}$ filtration efficiency of the electrospun nanofiber filter fabricated with or without the electrolyte solution. The calculated QF values were 0.1323 ± 0.0114 , 0.1213 ± 0.0112 , 0.1053 ± 0.0064 , and 0.0794 ± 0.0041 Pa $^{-1}$ for SAEN-NY, SAEN-PCL/GEL, SAEN-PVDF, and SAEN-PS filter on the fabric mesh, respectively. These values were similar to or larger than the QF range of KF94 mask (0.0989–0.1189 Pa $^{-1}$). Especially, the SAEN-NY filter showed the highest QF among other SAEN filters or KF94 mask. Data of P and Δp for the calculation of QF was shown in Table S1.

Air permeability is another essential factor in the performance of numerous devices, including medical patches, clothing, and air filters. Since electrospun nanofiber filters and SAEN filters were deposited onto the fabric mesh, their air permeability was lower than that of fabric mesh, as shown in Fig. 6d. The air permeability of SAEN-NY, SAEN-PCL/GEL, SAEN-PVDF, SAEN-PS filters were 10.09 ± 0.96 , 9.73 ± 2.49 , 14.83 ± 1.20 , and 11.63 ± 2.51 cm s $^{-1}$, respectively. Considering that the air permeability of KF94 mask was 10.16 ± 0.55 cm s $^{-1}$, all SAEN filters possessed similar or higher air permeability than KF94 mask. Furthermore, airflow also plays a significant role in the PM filtration efficiency, pressure drop, and QF of air filters. Generally, as airflow velocity increases, the filtration efficiency decreases, and pressure drop increases. In Fig. 6e, $PM_{2.5}$ filtration efficiency and pressure drop of electrospun nanofiber filters and SAEN filters made of four different polymers followed a general tendency of pressure drop according to the velocity change of airflow. However, since the change of pressure drop has a greater effect on QF than the filtration efficiency, QF values of SAEN filters could be decreased as the velocity

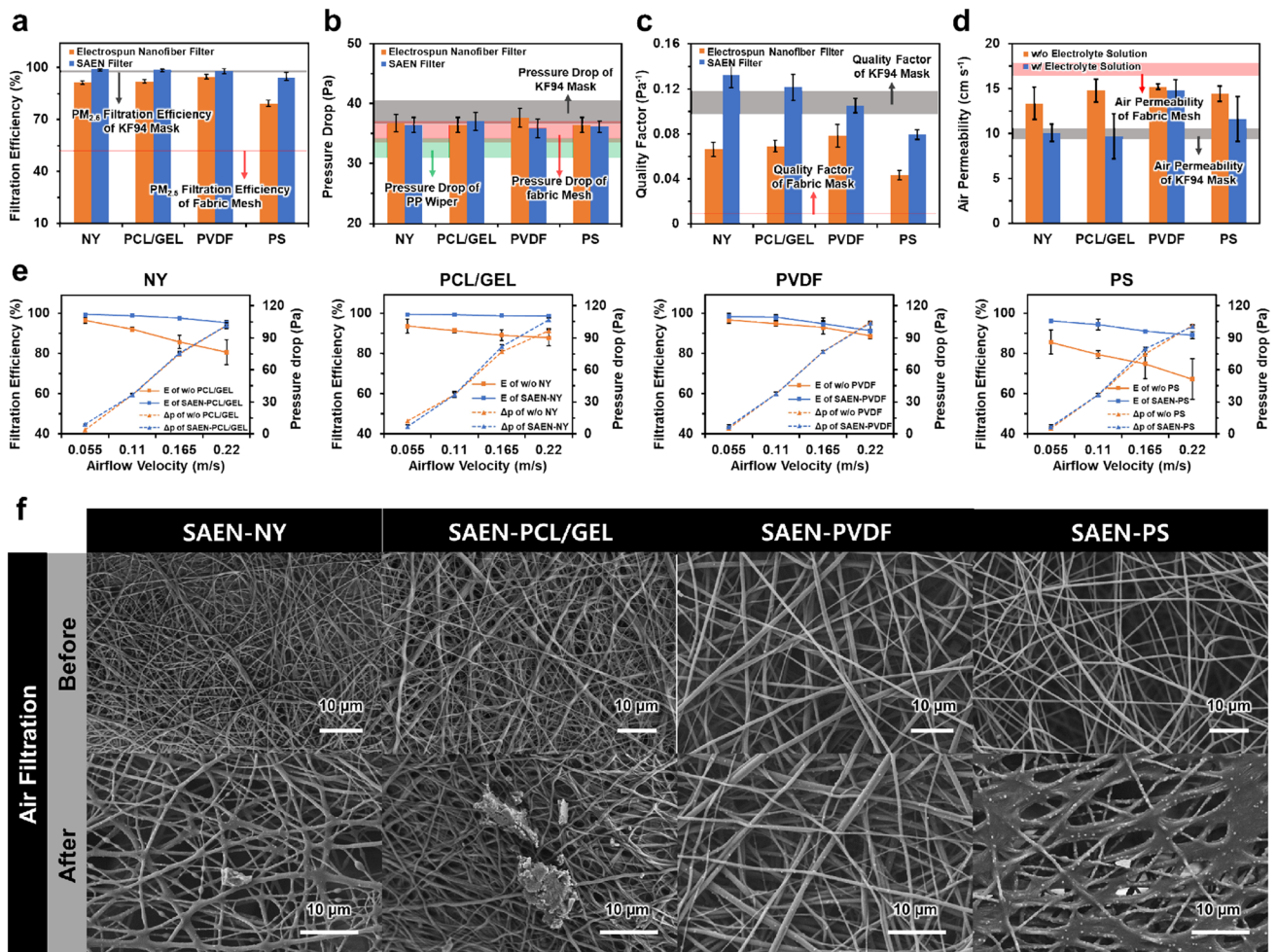


Fig. 6 PM_{2.5} filtration efficiency (a), pressure drop (b), quality factor (QF) (c), Air permeability (d), and change of PM_{2.5} filtration efficiency and pressure drop under different airflow velocities (e) of four different SAEN filters and electrospun nanofiber fabri-

cated without the electrolyte solution compared to fabric mesh and the KF94 mask. **f** Magnified SEM images of PM non-filtered and PM filtered SAEN filters made of four different polymers. All scale bars are 10 μm

of airflow increases, as shown in Fig. S2. The morphology of SAEN filters before and after air filtration is illustrated in Fig. 6f. As expected from the self-assembled structure of SAEN filters with similar or higher PM_{2.5} filtration efficiency compared with commercial masks, each SAEN filter could capture PM_{2.5} and below by adhesion and sieving with self-assembled electrospun nanofibers. Given its high PM_{2.5} filtration efficiency and QF with considerable air permeability compared with the KF94 mask, the SAEN filter appeared effective as a filter.

The SAEN filters were further characterized using small PM sized below 1.0 μm or 0.5 μm. As exhibited in Fig. 7a, the PM_{1.0} filtration efficiency of all SAEN filters was within the range of that of KF94 mask. In Fig. 7b, the SAEN-NY filter showed 20% higher PM_{0.5} filtration efficiency than KF94 mask and was more effective than other SAEN filters in terms of PM_{0.5} filtration. Considering that

PM_{1.0} and PM_{0.5} were simultaneously counted with PM_{2.5} by PM sensors, the pressure drop would have been the same during the measurement of PM_{2.5}, PM_{1.0}, and PM_{0.5}, as shown in Fig. 7b. Thereby, QF could be calculated by PM_{1.0} and PM_{0.5} filtration efficiency because QF is the function expressed by the filtration efficiency and the pressure drop. The assumption was that the QF of all SAEN filters was similar to or higher than that of KF94 mask under the same experimental environment, indicating that the performance of all SAEN filters was comparable with or more effective than that of KF94 mask. Given that daily air filter masks are widely consumed because of pathogens, such as COVID-19, or increasingly serious air pollution, a tremendous amount of these materials have been discarded due to challenges of reuse or recycling, significantly harming the environment. Here, the repetitive fabrication and detachment of the SAEN filter on a single fabric mask was

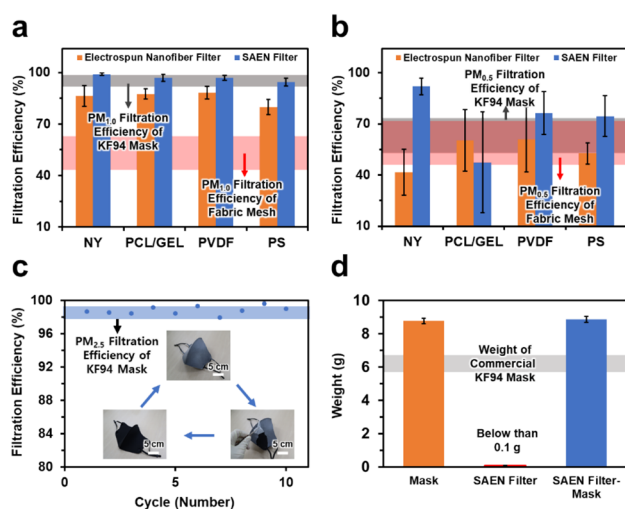


Fig. 7 $PM_{1.0}$ (a) and $PM_{0.5}$ (b) filtration efficiency of SAEN filters and electrospun nanofiber filters fabricated without the electrolyte solution. c $PM_{2.5}$ filtration efficiency of the SAEN filter under the repetitive cycle of fabrication, use, and detachment. Inset of c: the image of the repetitive cycle of the fabrication, use, and detachment of the SAEN filter on a single fabric filter. Scale bars are 5 cm. d Base weight of the mask, the SAEN filter, and the SAEN filter with a fabric mask

studied as a solution for mask waste reduction. The SAEN filter, which played a critical role in the air filtration, was repetitively fabricated and detached after being used. Generally, deposited nanofibers cannot retain their shape and morphology when reunited after detachment from the collector, making it difficult to reuse the SAEN filter after separation. However, the separated fabric mask for the mechanical support of the SAEN filter could be reused, as shown in the inset of Fig. 7c. Air filtration tests of the repetitively fabricated SAEN filters on a fabric mask revealed their effective $PM_{2.5}$ filtration efficiency comparable with that of KF94 mask (Fig. 7c). Furthermore, the detached SAEN filter weighed only around 0.08 g, which is 1% of the mass of KF94 mask (Fig. 7d). In consideration of the waste of commercial masks, SAEN filters are expected to reduce the waste generated by disposable masks in daily life.

With PP wiper adopted as another substrate, the $PM_{2.5}$ filtration efficiency was compared between SAEN filters and electrospun nanofiber filters fabricated without the electrolyte solution to confirm the applicability of SAEN filter fabrication to other substrates (Fig. S3). The $PM_{2.5}$ efficiency of SAEN-NY, SAEN-PCL/GEL, and SAEN-PS filter increased by 18%, 14%, and 28%, respectively, compared with that of electrospun nanofiber filters fabricated without the electrolyte solution even on PP wipers. Moreover, the SAEN-NY filter showed the highest $PM_{2.5}$ filtration

efficiency ($99.19 \pm 0.11\%$) and had a similar performance to the SAEN-NY filter on the fabric mesh, indicating that the $PM_{2.5}$ filtration performance of the SAEN-NY filter is effective even on the PP wiper. The SAEN-NY filter showed the highest $PM_{2.5}$ filtration efficiency and QF value regardless of the substrate. Thus, the SAEN-NY filter could be applied as the dual-functional SAEN filter that could simultaneously capture PM and sense formaldehyde gas.

For in-depth investigation, a numerical simulation of airflow through the SAEN filter and the electrospun nanofiber filter fabricated without the electrolyte solution was performed, as shown in Fig. S4a. In Fig. S4a-(i), the velocity profile along the reference line $l(x)$ showed that the airflow was highly concentrated to the thin part of the electrospun nanofiber filter fabricated without the electrolyte solution. In general, thin parts of electrospun nanofiber filters could diminish filtration efficiency. The electrospun nanofiber filter fabricated onto the non-conductive mesh collector without the electrolyte solution had many locally thin parts with small numbers of nanofibers and thus could allow most airflow to pass through them. Thus, the PM in the airflow passing through relatively thin parts was not sufficiently filtered through sieving and adhesion, leading to the low filtration efficiency of the electrospun nanofiber filter. By contrast, a constant velocity profile, which is close to the initial setting speed, was observed through the SAEN filter in Fig. S4a-(ii). Comparison between the velocity of the electrospun nanofiber filter fabricated without the electrolyte solution and SAEN filter is shown in Fig. S4b. On the basis of $PM_{2.5}$ filtration experiments and simulation results, the SAEN filter could perform more stable PM filtration than the electrospun nanofiber filter fabricated without the electrolyte solution.

Colorimetric Formaldehyde Sensing by Dual-Functional SAEN Filter

Another major cause of air pollution is VOCs, which can cause mild pain or even death depending on the type of compound and the amount of exposure. Half-face or full-face respirators with high VOC removal rates, similar to 95% $PM_{2.5}$ filtration efficiency from disposable masks, have been widely employed. However, their usage is inconvenient for daily life because the VOC absorption function is only achieved when the respirators are equipped properly. In addition, respirators or gas absorbers have been limited to higher VOC concentrations than allowable gas concentrations. Given that small amounts of VOC could harm people, individuals would already be exposed to the potential risk when they could not recognize the high levels of VOCs. In this regard, VOC gas sensing and alarming would be an effective way to determine the existence of the VOC and avoid the danger of the VOC. In this study, the dual-functional SAEN filter on the mask would detect formaldehyde gas

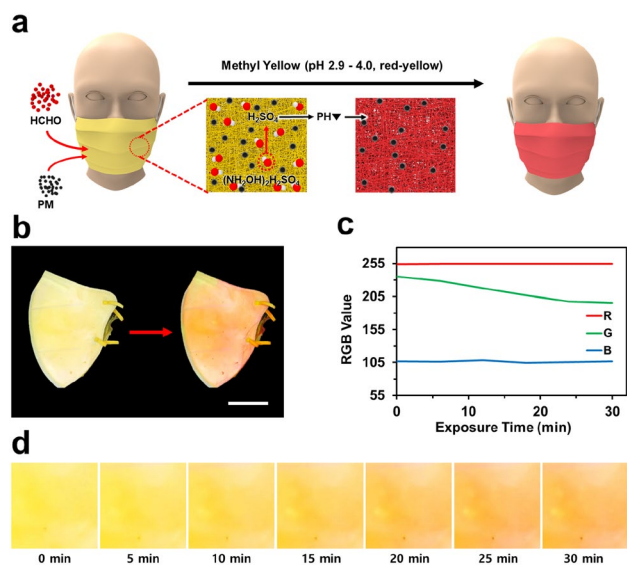


Fig. 8 **a** Schematic diagram of formaldehyde gas sensing with the dual-functional SAEN filter on the mask. **b** Yellow-to-red color changing of the dual-functional SAEN filter through exposure to formaldehyde gas. The scale bar is 5 cm. The RGB values from captured images (**c**) and photographs (**d**) presented the yellow to red color change of the dual-functional SAEN filter upon exposure to 5 ppm formaldehyde gas for 30 min

and notify the existence of the formaldehyde gas according to its eye-readable color change. Among VOCs, formaldehyde, a representative indoor VOC, is colorless and indistinguishable from the naked eye and is generally emitted from wooden floors, decorative paints, furniture, and cosmetics. Long-term exposure to formaldehyde would cause serious health problems, including skin rashes, shortness of breath, wheezing and changes in lung function, and even underlying death [77, 78]. Although nanofiber-based VOC gas sensors have been reported, the sequential process of electrospinning and chemical treatment is required to achieve VOC gas sensing functionalities [66, 79].

In this study, the one-step fabrication of a dual-functional SAEN filter for both PM removal and colorimetric formaldehyde gas sensing was achieved by conducting electrospinning with the electrolyte solution possessing a formaldehyde-sensitive colorimetric agent as a collector (Fig. 8a). The colorimetric formaldehyde gas sensing function of the dual-functional SAEN filter can be explained as follows. First, the hydroxylamine in the dual-functional SAEN filter reacts with formaldehyde gas in the air, forming an acid and decreasing pH. Second, the change in the pH alters the color from yellow to red due to the presence of methyl yellow in the dual-functional SAEN filter, and this change could be detected by the naked eye (Fig. 8b). For the quantitative evaluation of the color change of the dual-functional SAEN filter, the RGB values of the image of the dual-functional SAEN filter with respect to exposure time are shown in

Fig. 8c. Red and blue values were almost fixed at around 255 and 105, respectively, but the green value decreased when the exposure time of formaldehyde gas increased. Hence the color of the dual-functional SAEN filter changed from yellow to red. The time-lapse image of the dual-functional SAEN filter under formaldehyde gas is shown in Fig. 8d. The exposure to formaldehyde gas induced the substantial color change of the dual-functional SAEN filter from yellow to red, demonstrating onsite and eye-readable formaldehyde detection.

The effectiveness of the dual-functional SAEN filter was further evaluated with different concentrations of formaldehyde gas and times after fabrication, as shown in Fig. 9a, b. As the formaldehyde gas concentration increased, the red and blue values were kept constant, and the green values decreased, which demonstrated the possibility of measuring the exact concentration of the formaldehyde gas by evaluating color change (Fig. 9a). After storing the fabricated dual-functional SAEN filters for 1, 2, and 3 weeks, dual-functional SAEN filters showed similar color change for 30 min at a 5 ppm concentration of formaldehyde gas, and thus the dual-functional SAEN filter could be effective for detecting formaldehyde gas without significant performance change for at least 3 weeks (Fig. 9b). In Fig. 9c, the morphology of dual-functional SAEN filter after PM filtration, the formaldehyde gas reaction, and a sequential combination of the two processes was exhibited to demonstrate the morphology change of the dual-functional SAEN filter. SEM images of four cases confirmed the morphology changes of the SAEN filter when adding the formaldehyde gas reaction. Furthermore, PM_{2.5} filtration efficiency, pressure drop, quality factor, and color change of dual-functional SAEN filters with different exposure times were evaluated, as displayed in Fig. 9d. The PM_{2.5} filtration efficiency and pressure drop slightly changed due to the morphological change by formaldehyde gas reaction, which can contribute to enlarging the surface area to sieving and adhesion for PM and suppressing the airflow causing the decrease of pressure drop. As a result, the QF value also slightly changed due to the relationship between PM_{2.5} filtration efficiency and pressure drop for QF calculation. However, QF values of dual-functional SAEN filter after formaldehyde gas detection were slightly degraded and maintained a high value compared to a KF94 mask.

On the basis of all experimental and simulated results, the fabricated dual-functional SAEN filters are effective for simultaneous PM filtration and sensing formaldehyde gas in practical use. This fabrication process could be applied for highly efficient and practical applications that deal with complex air pollution.

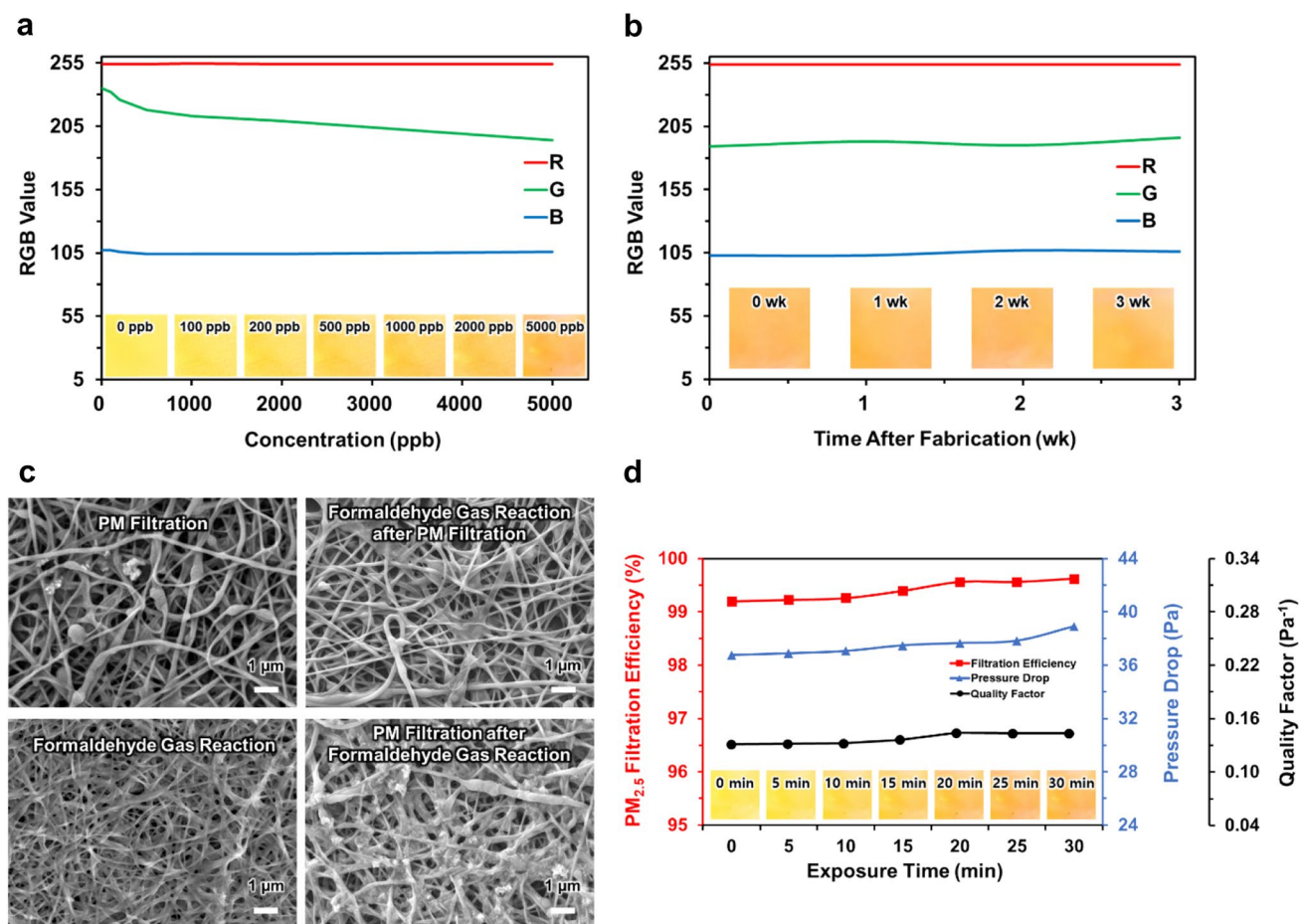


Fig. 9 The RGB values from captured images by different concentrations (0, 100, 200, 500, 1,000, 2,000, and 5,000 ppb for 30 min) (a) and time after fabrication (1, 2, and 3 weeks) (b). c SEM images of dual-functional SAEN filter after PM filtration, after formaldehyde

gas reaction, and after a combination of the two processes. All scale bars are 1 μm . d PM_{2.5} filtration efficiency, pressure drop, quality factor, and color change of dual-functional SAEN filters with different exposure times

Conclusion

In summary, a one-step fabrication of dual-functional SAEN filters for PM filtration, and detection of formaldehyde gas was demonstrated as a facile strategy. SAEN filters were directly deposited onto the non-conductive mesh collector with uniform deposition and exhibited high PM_{2.5} filtration efficiency. In addition, the SAEN filter could facilitate the permeation of airflow similar to the commercial masks, resulting in a high QF, and could be fabricated with uniform deposition even onto the PP wiper with high PM_{2.5} filtration efficiency. Small PM below 1.0 or 0.5 μm was also captured by the SAEN filter, resulting in its higher PM_{1.0} and PM_{0.5} filtration efficiency than the commercial mask. Meanwhile, a repeated cycle of the fabrication, use, and detachment of the SAEN filter on a single fabric mask was developed by discarding only the SAEN filter and reusing the fabric mask. As a result, the waste was dramatically reduced compared with that when using a commercial air filter mask.

The PM_{2.5} filtration efficiency of the SAEN filter on a single fabric mask was higher than that of commercial masks but did not decrease with repeated fabrication and detachment. Finally, during electrospinning, the formaldehyde-sensitive agents were impregnated into the SAEN filter. Thus, the dual-functional SAEN filter was fabricated for PM removal and formaldehyde gas sensing. Gradual colorimetric change in response to formaldehyde gas was detected on the site in an eye-readable manner. Owing to the severity and complexity of air pollution and the diversification of its causes, this one-step fabrication of dual-functional SAEN filters would provide numerous opportunities for various applications in individual respiratory protection and indoor facility purification.

Supplementary Information The online version contains supplementary material available at <https://doi.org/10.1007/s42765-023-00279-3>.

Acknowledgements This work was supported by the National Research Foundation of Korea (NRF) grant funded by the Korea government

(MSIT) (no. RS-2023-00209094, 2020R1C1C100944311) and BK21 FOUR Program by Pusan National University Research Grant, 2021. Jin Yeong Song is grateful for financial support from Hyundai Motor Chung Mong-Koo Foundation.

Data Availability The data that support the findings of this study are available from the authors upon reasonable request.

Declarations

Conflict of interest The author state that there are no conflicts of interest to disclose.

References

- Brunekreef B, Holgate ST. Air pollution and health. *The Lancet*. **2002**;360:1233.
- Kampa M, Castanas E. Human health effects of air pollution. *Environ Pollut*. **2008**;151:362.
- Van de Velde M, Schepers R, Berends N, Vandermeersch E, De Buck F. Ten years of experience with accidental dural puncture and post-dural puncture headache in a tertiary obstetric anaesthesia department. *Int J Obstet Anesth*. **2008**;17:329.
- Snyder EG, Watkins TH, Solomon PA, Thoma ED, Williams RW, Hagler GSW, Shelow D, Hindin DA, Kilaru VJ, Preuss PW. The changing paradigm of air pollution monitoring. *Environ Sci Technol*. **2013**;47:11369.
- Glencross DA, Ho TR, Camina N, Hawrylowicz CM, Pfeffer PE. Air pollution and its effects on the immune system. *Free Radic Biol Med*. **2020**;151:56.
- Gonzalez-Martín J, Kraakman NJR, Perez C, Lebrero R, Muñoz R. A state-of-the-art review on indoor air pollution and strategies for indoor air pollution control. *Chemosphere*. **2021**;262: 128376.
- Hamanaka RB, Mutlu GM. Particulate matter air pollution: effects on the cardiovascular system. *Front Endocrinol*. **2018**;9:680.
- Daellenbach KR, Uzu G, Jiang J, Cassagnes LE, Leni Z, Vlachou A, Stefanelli G, Canonaco F, Weber S, Segers A, Kuenen JJP, Schaap M, Favez O, Albinet A, Aksoyoglu S, Dommen J, Baltensperger U, Geiser M, Haddad IE, Jaffrezo JL, Prevot ASH. Sources of particulate-matter air pollution and its oxidative potential in Europe. *Nature*. **2020**;587:414.
- Lee BJ, Kim B, Lee K. Air pollution exposure and cardiovascular disease. *Toxicol Res*. **2014**;30:71.
- Møhlhave L. Organic compounds as indicators of air pollution. *Indoor Air*. **2002**;13:12.
- Salthammer T. Very volatile organic compounds: an understudied class of indoor air pollutants. *Indoor Air*. **2016**;26:25.
- Dominici F, Greenstone M, Sunstein CR. Particulate Matter Matters. *Science*. **2014**;334:257.
- Zhang R, Wang G, Guo S, Zamora ML, Ying Q, Lin Y, Wang W, Hu M, Wang Y. Formation of urban fine particulate matter. *Chem Rev*. **2015**;115:3803.
- Mukherjee A, Agrawal M. World air particulate matter: sources, distribution and health effects. *Environ Chem Lett*. **2017**;15:283.
- Atkinson R, Arey J. Atmospheric degradation of volatile organic compounds. *Chem Rev*. **2003**;103:4605.
- Kamal MS, Razzak SA, Hossain MM. Catalytic oxidation of volatile organic compounds (VOCs)—a review. *Atmos Environ*. **2016**;140:117.
- Liu H, Cao C, Huang J, Chen Z, Chen G, Lai Y. Progress on particulate matter filtration technology: basic concepts, advanced materials, and performances. *Nanoscale*. **2020**;12:437.
- Valencia-Osorio LM, Álvarez-Láinez ML. Global view and trends in electrospun nanofiber membranes for particulate matter filtration: a review. *Macromol Mater Eng*. **2021**;306:2100278.
- Ji X, Huang J, Teng L, Li S, Li X, Cai W, Chen Z, Lai Y. Advances in particulate matter filtration: materials, performance, and application. *Green Energy Environ*. **2022** (in press).
- Iranpour R, Cox HHJ, Deshusses MA, Schroeder ED. Literature review of air pollution control biofilters and biotrickling filters for odor and volatile organic compound removal. *Environ Prog*. **2005**;24:254.
- Berenjian A, Chan N, Malmiri HJ. Volatile organic compounds removal methods: a review. *Am J Biochem Biotechnol*. **2012**;8:220.
- McGinn CK, Lamport ZA, Kymissis I. Review of gravimetric sensing of volatile organic compounds. *ACS Sens*. **2020**;5:1514.
- Matuschek C, Moll F, Fangerau H, Fischer JC, Zanker K, van Griensven M, Schneider M, Kindgen-Milles D, Knoefel WT, Lichtenberg A, Tamaskovics B, Djiepmo-Njanang FJ, Budach W, Corradini S, Haussinger D, Feldt T, Jensen B, Pelka R, Orth K, Peiper M, Grebe O, Maas K, Bolke E, Haussmann J. The history and value of face masks. *Eur J Med Res*. **2020**;25:23.
- Adanur S, Jayswal A. Filtration mechanisms and manufacturing methods of face masks: an overview. *J Ind Text*. **2020**;51:3683S.
- Bognitzki M, Czado W, Frese T, Schaper A, Hellwig M, Steinhart M, Greiner A, Wendorff JH. Nanostructured fibers via electrospinning. *Adv Mater*. **2001**;13:70.
- Li D, Xia Y. Electrospinning of nanofibers: reinventing the wheel? *Adv Mater*. **2004**;16:1151.
- Ryu HI, Koo MS, Kim S, Kim S, Park YA, Park SM. Uniform-thickness electrospun nanofiber mat production system based on real-time thickness measurement. *Sci Rep*. **2020**;10:20847.
- Song JY, Ryu HI, Lee JM, Bae SH, Lee JW, Yi CC, Park SM. Conformal fabrication of an electrospun nanofiber mat on a 3D ear cartilage-shaped hydrogel collector based on hydrogel-assisted electrospinning. *Nanoscale Res Lett*. **2021**;16:116.
- Han KS, Lee S, Kim M, Park P, Lee MH, Nah J. Electrically activated ultrathin PVDF-TrFE air filter for high-efficiency PM_{1.0} filtration. *Adv Funct Mater*. **2019**;29:1903633.
- Lakshmanan A, Gavali DS, Venkataprasanna KS, Thapa R, Sarkar D. Low-basis weight polyacrylonitrile/polyvinylpyrrolidone blend nanofiber membranes for efficient particulate matter capture. *ACS Appl Polym Mater*. **2022**;4:3971.
- Reddy MV, Julien CM, Mauger A, Zaghbi K. Sulfide and oxide inorganic solid electrolytes for all-solid-state li batteries: a review. *Nanomaterials*. **2020**;10:1606.
- Zhang R, Liu C, Hsu PC, Zhang C, Liu N, Zhang J, Lee HR, Lu Y, Qiu Y, Chu S, Cui Y. Nanofiber air filters with high-temperature stability for efficient PM_{2.5} removal from the pollution sources. *Nano Lett*. **2016**;16:3642.
- Souzandeh H, Scudiero L, Wang Y, Zhong WH. A disposable multi-functional air filter: paper towel/protein nanofibers with gradient porous structures for capturing pollutants of broad species and sizes. *ACS Sustain Chem Eng*. **2017**;5:6209.
- Zhang R, Liu B, Yang A, Zhu Y, Liu C, Zhou G, Sun J, Hsu PC, Zhao W, Lin D, Liu Y, Pei A, Xie J, Chen W, Xu J, Jin Y, Wu T, Huang X, Cui Y. In situ investigation on the nanoscale capture and evolution of aerosols on nanofibers. *Nano Lett*. **2018**;18:1130.
- Zhang S, Liu H, Tang N, Ali N, Yu J, Ding B. Highly efficient, transparent, and multifunctional air filters using self-assembled 2D nanoarchitected fibrous networks. *ACS Nano*. **2019**;13:13501.
- Lee S, Cho AR, Park D, Kim JK, Han KS, Yoon IJ, Lee MH, Nah J. Reusable polybenzimidazole nanofiber membrane filter for highly breathable PM_{2.5} dust proof mask. *ACS Appl Mater Interfaces*. **2019**;11:2750.
- Bian Y, Wang S, Zhang L, Chen C. Influence of fiber diameter, filter thickness, and packing density on PM_{2.5} removal efficiency

- of electrospun nanofiber air filters for indoor applications. *Build Environ.* **2020**;170:106628.
38. Zhang S, Liu H, Tang N, Zhou S, Yu J, Li B, Ding B. Spiderweb-inspired PM0.3 filters based on self-sustained electrostatic nanostructured networks. *Adv Mater.* **2020**;32:2002361.
 39. Cui J, Wang Y, Lu T, Liu K, Huang C. High performance, environmentally friendly and sustainable nanofiber membrane filter for removal of particulate matter 1.0. *J Colloid Interface Sci.* **2021**;597:48.
 40. Xu J, Liu C, Hsu PC, Liu K, Zhang R, Liu Y, Cui Y. Roll-to-roll transfer of electrospun nanofiber film for high-efficiency transparent air filter. *Nano Lett.* **2016**;16:1270.
 41. Zuo F, Zhang S, Liu H, Fong H, Yin X, Yu J, Ding B. Free-standing polyurethane nanofiber/nets air filters for effective PM capture. *Small.* **2017**;13:1702139.
 42. Cheng Z, Cao J, Kang L, Luo Y, Li T, Liu W. Novel transparent nano-pattern window screen for effective air filtration by electrospinning. *Mater Lett.* **2018**;221:157.
 43. Wang X, Xiang H, Song C, Zhu D, Sui J, Liu Q, Long Y. Highly efficient transparent air filter prepared by collecting-electrode-free bipolar electrospinning apparatus. *J Hazard Mater.* **2020**;385: 121535.
 44. Xiong J, Shao W, Wang L, Cui C, Gao Y, Jin Y, Yu H, Han P, Liu F, He J. High-performance anti-haze window screen based on multiscale structured polyvinylidene fluoride nanofibers. *J Colloid Interface Sci.* **2022**;607:711.
 45. Zhang S, Liu H, Tang N, Ge J, Yu J, Ding B. Direct electrospinning of high-performance membranes based on self-assembled 2D nanoarchitected networks. *Nat Commun.* **2019**;10:1458.
 46. Park SM, Kim DS. Electrolyte-assisted electrospinning for a self-assembled, free-standing nanofiber membrane on a curved surface. *Adv Mater.* **2015**;27:1682.
 47. Park SM, Eom S, Kim W, Kim DS. Role of grounded liquid collectors in precise patterning of electrospun nanofiber mats. *Langmuir.* **2018**;34:284.
 48. Park SM, Eom S, Choi D, Han SJ, Park SJ, Kim DS. Direct fabrication of spatially patterned or aligned electrospun nanofiber mats on dielectric polymer surfaces. *Chem Eng J.* **2018**;335:712.
 49. Li CC. Aerodynamic behavior of a gas mask canister containing two porous media. *Chem Eng Sci.* **1832**;2009:64.
 50. Su YC, Li CC. Computational fluid dynamics simulations and tests for improving industrial-grade gas mask canisters. *Adv Mech Eng.* **2015**;7:1687814015596297.
 51. Tcharkhtchi A, Abbasnezhad N, Zarbini Seydani M, Zirak N, Farzaneh S, Shirinbayan M. An overview of filtration efficiency through the masks: mechanisms of the aerosols penetration. *Bioact Mater.* **2021**;6:106.
 52. Floyd EL, Henry JB, Johnson DL. Influence of facial hair length, coarseness, and areal density on seal leakage of a tight-fitting half-face respirator. *J Occup Environ Hyg.* **2018**;15:334.
 53. Regli A, Sommerfield A, von Ungern-Sternberg BS. The role of fit testing N95/FFP2/FFP3 masks: a narrative review. *Anaesthesia.* **2021**;76:91.
 54. Bollinger N. NIOSH respirator selection logic. Cincinnati: DHHS (NIOSH); 2004. p. 2–15.
 55. Hodgkinson J, Tatam RP. Optical gas sensing: a review. *Meas Sci Technol.* **2013**;24: 012004.
 56. Feng S, Farha F, Li Q, Wan Y, Xu Y, Zhang T, Ning H. Review on smart gas sensing technology. *Sensors.* **2019**;19:3670.
 57. Ji H, Zeng W, Li Y. Gas sensing mechanisms of metal oxide semiconductors: a focus review. *Nanoscale.* **2019**;11:22664.
 58. Reddy K, Guo Y, Liu J, Lee W, Khaing Oo MK, Fan X. Rapid, sensitive, and multiplexed on-chip optical sensors for micro-gas chromatography. *Lab Chip.* **2012**;12:901.
 59. Oh SY. Fast gas chromatography–surface acoustic wave sensor: an effective tool for discrimination and quality control of Lavandula species. *Sens Actuator B-Chem.* **2013**;182:223.
 60. van den Broek J, Abegg S, Pratsinis SE, Guntner AT. Highly selective detection of methanol over ethanol by a handheld gas sensor. *Nat Commun.* **2019**;10:4220.
 61. Kim YK, Hwang SH, Jeong SM, Son KY, Lim SK. Colorimetric hydrogen gas sensor based on PdO/metal oxides hybrid nanoparticles. *Talanta.* **2018**;188:356.
 62. Kang K, Park J, Kim B, Na K, Cho I, Rho J, Yang D, Lee JY, Park I. Self-powered gas sensor based on a photovoltaic cell and a colorimetric film with hierarchical micro/nanostructures. *ACS Appl Mater Interfaces.* **2020**;12:39024.
 63. Cho SH, Suh JM, Eom TH, Kim T, Jang HW. Colorimetric sensors for toxic and hazardous gas detection: a review. *Electron Mater Lett.* **2020**;17:1.
 64. Nakano N, Ishikawa M, Kooabayashi Y, Nagashima K. Development of a monitoring tape for formaldehyde using hydroxylamine sulfate and methyl yellow. *Anal Sci.* **1994**;10:641.
 65. Wang X, Si Y, Wang J, Ding B, Yu J, Al-Deyab SS. A facile and highly sensitive colorimetric sensor for the detection of formaldehyde based on electro-spinning/netting nano-fiber/nets. *Sens Actuator B-Chem.* **2012**;163:186.
 66. Kim DH, Cha JH, Lim JY, Bae J, Lee W, Yoon KR, Kim C, Jang JS, Hwang W, Kim ID. Colorimetric dye-loaded nanofiber yarn: eye-readable and weavable gas sensing platform. *ACS Nano.* **2020**;14:16907.
 67. Song JY, Oh JH, Choi D, Park SM. Highly efficient patterning technique for silver nanowire electrodes by electro-spray deposition and its application to self-powered triboelectric tactile sensor. *Sci Rep.* **2021**;11:21437.
 68. Jeong S, Cho H, Han S, Won P, Lee H, Hong S, Yeo J, Kwon J, Ko SH. High efficiency, transparent, reusable, and active PM_{2.5} filters by hierarchical ag nanowire percolation network. *Nano Lett.* **2017**;17:4339.
 69. Ding B, Wang M, Wang X, Yu J, Sun G. Electrospun nanomaterials for ultrasensitive sensors. *Mater Today.* **2010**;13:16.
 70. Wang X, Ding B, Yu J, Wang M, Pan F. A highly sensitive humidity sensor based on a nanofibrous membrane coated quartz crystal microbalance. *Nanotechnology.* **2010**;21: 055502.
 71. Wang X, Ding B, Yu J, Si Y, Yang S, Sun G. Electro-netting: fabrication of two-dimensional nano-nets for highly sensitive trimethylamine sensing. *Nanoscale.* **2011**;3:911.
 72. Zhao S, Zhou Q, Long YZ, Sun GH, Zhang Y. Nanofibrous patterns by direct electrospinning of nanofibers onto topographically structured non-conductive substrates. *Nanoscale.* **2013**;5:4993.
 73. Jia C, Yu D, Lamarre M, Leopold PL, Teng YD, Wang H. Patterned electrospun nanofiber matrices via localized dissolution: potential for guided tissue formation. *Adv Mater.* **2014**;26:8192.
 74. Li D, Ouyang G, McCann JT, Xia Y. Collecting electrospun nanofibers with patterned electrodes. *Nano Lett.* **2005**;5:913.
 75. Wu Y, Dong Z, Wilson S, Clark RL. Template-assisted assembly of electrospun fibers. *Polymer.* **2010**;51:3244.
 76. Kolářová K, Vosmanská V, Rimpelová S, Švorčík V. Effect of plasma treatment on cellulose fiber. *Cellulose.* **2013**;20:953.
 77. Fasth IM, Ulrich NH, Johansen JD. Ten-year trends in contact allergy to formaldehyde and formaldehyde-releasers. *Contact Dermatitis.* **2018**;79:263.
 78. Liu C, Miao X, Li J. Outdoor formaldehyde matters and substantially impacts indoor formaldehyde concentrations. *Build Environ.* **2019**;158:145.
 79. Horzum N, Tascioglu D, Özbek C, Okur S, Demir MM. VOC sensors based on a metal oxide nanofibrous membrane/QCM system prepared by electrospinning. *New J Chem.* **2014**;38:5761.

Publisher's Note Springer Nature remains neutral with regard to jurisdictional claims in published maps and institutional affiliations.

Springer Nature or its licensor (e.g. a society or other partner) holds exclusive rights to this article under a publishing agreement with the author(s) or other rightsholder(s); author self-archiving of the accepted manuscript version of this article is solely governed by the terms of such publishing agreement and applicable law.



Jin Yeong Song is currently pursuing a M.S. under the supervision of Prof. Sang Min Park, Pusan National University. He started his academic studies in the field of Mechanical Engineering and received a B.S. degree from Pusan National University, South Korea, in 2021. His research interest is based on 2D and 3D conformal electrospinning and its environmental applications for electrospun nanofiber air filters.



Seongmin Kim received a B.S. under the supervision of Prof. Sang Min Park from Pusan National University, South Korea, in 2021. He started his academic studies in the field of Mechanical Engineering from Pusan National University, South Korea. His research interest is based on fabricating technology of transparent electrodes and strain sensors.



Jaeseong Park is currently pursuing a B.S. under the supervision of Prof. Youngsoo Kim, Pusan National University. He started his academic studies in the field of Mechanical Engineering from Pusan National University, South Korea. His research interest is based on kinematics-based mechanism modeling and simulation.



Sang Min Park is an assistant professor at the School of Mechanical Engineering, Pusan National University, South Korea. He received his Ph.D. degree from Pohang University of Science and Technology (POSTECH) in 2018, by developing an electrolyte-assisted electrospinning technique for recapitulating the blood-tissue interfaces. His research is focusing the development of advanced nano/microfabrication techniques, including lithography, 3D printing, electrospinning,

electrospray, and multi-scale production system based on artificial intelligence. Details can be found <https://sites.google.com/view/ipmslab/>.